Acta Biomaterialia 92 (2019) 229–240

Contents lists available at ScienceDirect

Acta Biomaterialia

journal homepage: www.elsevier.com/locate/actabiomat

Full length article

Co-administration of combretastatin A4 nanoparticles and sorafenib for systemic therapy of hepatocellular carcinoma

Yalin Wang [a,b], Haiyang Yu [b,c], Dawei Zhang [b], Guanyi Wang [b], Wantong Song [b,c], Yingmin Liu [a], Sheng Ma [b,c], Zhaohui Tang [b,c,*], Ziling Liu [a,*], Kazuo Sakurai [d], Xuesi Chen [b,c]

[a] Cancer Center, the First Hospital of Jilin University, Changchun 130021, China
[b] Key Laboratory of Polymer Ecomaterials, Changchun Institute of Applied Chemistry, Chinese Academy of Sciences, Changchun 130022, China
[c] Jilin Biomedical Polymers Engineering Laboratory, Changchun 130022, China
[d] The University of Kitakyushu, Department of Chemistry and Biochemistry, 1-1, Hibikino, Wakamatsu-ku, Kitakyushu, Fukuoka 808-0135, Japan

ARTICLE INFO

Article history:
Received 8 January 2019
Received in revised form 7 May 2019
Accepted 9 May 2019
Available online 14 May 2019

Keywords:
CA4
Sorafenib
Hepatocellular carcinoma
Combination

ABSTRACT

Effective systemic therapy is highly desired for the treatment of hepatocellular carcinoma (HCC). In this study, a combination of nanoparticles of poly(L-glutamic acid)-*graft*-methoxy poly(ethylene glycol)/combretastatin A4 sodium salt (CA4-NPs) plus sorafenib is developed for the cooperative systemic treatment of HCC. The CA4-NPs leads to the disruption of established tumor blood vessels and extensive tumor necrosis, however, inducing increased expression of VEGF-A and angiogenesis. Sorafenib reduces the VEGF-A induced angiogenesis and further inhibits tumor proliferation, cooperating with the CA4-NPs. A significant decrease in tumor volume and prolonged survival time are observed in the combination group of CA4-NPs plus sorafenib compared with CA4-NPs or sorafenib monotherapy in subcutaneous and orthotopic H22 hepatic tumor models. Seventy-one percent of the mice are alive without residual tumor at 96 days post tumor inoculation for the subcutaneous models treated with CA4-NPs 30 or 35 $mg \cdot kg^{-1}$ plus sorafenib 30 $mg \cdot kg^{-1}$. Our findings suggest that co-administration of sorafenib and CA4-NPs possesses significant antitumor efficacy for HCC treatment.

Statement of Significance

Effective systemic therapy is highly desired for the treatment of hepatocellular carcinoma (HCC). Herein, we demonstrate that a combination of nanoparticles of poly(L-glutamic acid)-*graft*-methoxy poly(ethylene glycol)/combretastatin A4 sodium salt (CA4-NPs) plus sorafenib is a promising synergistic approach for systemic treatment of HCC. The CA4-NPs leads to the disruption of established tumor blood vessels and extensive tumor necrosis, however, inducing increased expression of VEGF-A and angiogenesis. Sorafenib reduces the VEGF-A induced angiogenesis and further inhibits tumor proliferation, cooperating with the CA4-NPs.

1. Introduction

Hepatocellular carcinoma (HCC) is the third leading cause of cancer-related death worldwide [1]. In China, the five-year age-standardized relative survival rate of liver cancer is the poorest of all cancers at only 10.2% [2]. As it is difficult to diagnose HCC early, a principle therapeutic challenge is management of its highly malignant features and rapid progression.

Surgical resection is the first therapeutic option for HCC. However, only 5–10% HCC patients (those with early-stage HCC) are suitable for this approach [3]. Most patients are diagnosed with HCC at an intermediate or advanced stage due to the insidious nature of symptom development with early-stage HCC. For patients

Abbreviations: HCC, hepatocellular carcinoma; TACE, transarterial chemoembolisation; CA4, combretastatin-A4; CA4-NPs, nanoparticles of poly(L-glutamic acid)-*graft*-methoxy poly(ethylene glycol)/combretastatin A4 sodium salt; VDAs, vascular disrupting agents; VEGF, vascular endothelial growth factor; EPR, enhanced permeability and retention; PLG-CA4, poly (L-glutamic acid)-*graft*-methoxy poly (ethylene glycol)/combretastatin A4; PLG-*g*-mPEG, Poly (L-glutamic acid)-*graft*-methoxy poly (ethylene glycol) copolymer; HRP, horseradish peroxidase; PBS, phosphate-buffered saline; IV, intravenous; IP, intraperitoneal; TSR, tumor suppression rate; AST, aspartate aminotransferase; ALT, alanine aminotransferase; BUN, blood urea nitrogen; MVD, microvascular density; SD, standard deviation.

* Corresponding authors at: Cancer Center, the First Hospital of Jilin University, Changchun 130021, China (Z. Liu); Key Laboratory of Polymer Ecomaterials, Changchun Institute of Applied Chemistry, Chinese Academy of Sciences, Changchun 130022, China (Z. Tang).

E-mail addresses: ztang@ciac.ac.cn (Z. Tang), ziling@jlu.edu.cn (Z. Liu).

https://doi.org/10.1016/j.actbio.2019.05.028
1742-7061/

with unresectable HCC, transarterial chemoembolization (TACE) or sorafenib is recommended. HCC is a highly vascularized tumor with abundant abnormal blood vessel development [4]. TACE is an important locoregional therapeutic approach to reduce vascular blood flow in intermediate stage HCC [5], where an anticancer drug injected through a catheter at the tumor site blocks the primary feeding artery of the tumor [6]. TACE increases tumor hypoxia and subsequent upregulation of vascular endothelial growth factor (VEGF), which might stimulate revascularisation and promote metastasis [7,8]. Sorafenib is a multikinase inhibitor that blocks tumor angiogenesis and HCC cell growth by inhibiting the RAF/MEK/ERK signal pathways and receptor tyrosine kinases. The latter includes vascular endothelial growth factor receptors 2 and 3 (VEGFR-2 and VEGFR-3, respectively), Flt-3, c-KIT, and platelet-derived growth factor receptor (PDGFR) [9,10]. Sorafenib has been widely used as a standard treatment of advanced HCC [11]. Therefore, it is reasonable to combine sorafenib with TACE to inhibit tumor proliferation and angiogenesis simultaneously for the synegistic treatment of HCC. Indeed, a recent randomised controlled phase II trial ('TACTICS') demonstrated that adding sorafenib to TACE significantly improved progression free survival in patients with unresectable HCC, compared with TACE alone at 25.2 versus 13.5 months, respectively (HR 0.59, 95% CI 0.41–0.87; $P = 0.006$). The TACTICS trial demonstrated that addition of sorafenib to TACE could improve clinical efficacy for patients with intermediate-stage HCC [12]. However, TACE is a locoregional therapeutic approach. It may not be easy for TACE to embolize the feeding arteries completely in patients with multifocal and massive HCC, which have abundant tumor-feeding arteries. In particular, TACE is not appropriate for advanced HCC with portal invasion and/or extrahepatic spread [3,13]. Furthermore, the intolerable complications of TACE such as hepatic failure and gastrointestinal hemorrhage limit the clinical application of TACE [14]. An effective alternative approach to TACE may be systemically administered agents that selectively reduce vascular in-flow in tumors. Therefore, we speculated that the combination of a systemically administered tumor blood-flow reducer plus sorafenib might be effective treatment for advanced (unresectable or metastatic) HCC.

Intravenous administration of vascular disrupting agents (VDAs) can selectively arrest tumor blood flow by disrupting the established tumor vasculature via targeting of endothelial cells [15–17]. VDAs produce much more blood-flow reduction in treated tumors than in normal tissues, and numerous clinical trials are ongoing with VDAs [18–20]. The difference in endothelial cells between tumors and normal tissues might contribute to the tumor susceptibility to VDAs [21,22]. These differences include proliferation rates, post-translational modifications of tubulin, tubulin mutations, types of microtubule-associated proteins and junctions between endothelial cells and pericytes. VDA treatment leads to extensive secondary necrosis due to ischemia in treated tumors [17,23–25]. This is similar to what occurs with TACE. Combretastatin-A4 (CA4) is a representative VDA. VDAs can cause significant central tumor necrosis while leaving a thin layer of viable tumor cells at the tumor periphery, which has high VEGF-A expression and promotes revascularisation and tumor regrowth [26–28]. VEGFR tyrosine kinase inhibitors can restrain the angiogenic activity of VEGF-A [29,30]. Therefore, the combination of a VEGFR tyrosine kinase inhibitor plus a VDA should be a promising approach for the treatment of HCC.

Nanomedicines have the advantage of long-term circulation and high drug accumulation in the tumor region owing to the enhanced permeability and retention (EPR) effect [31–33]. Recently, many drug delivery system targeting on tumor microenvironment have been designed for the treatment of cancer [34–36]. In previous work, we constructed a polymeric combretastatin-A4 [poly(L-glutamic acid)-*graft*-methoxy poly(ethylene glycol)/combretastatin A4, PLG-CA4] that was located mainly around tumor vessels after intravenous injection due to its low tissue penetration in solid tumors. This significantly enhanced the efficacy of CA4 in terms of solid tumor treatment as compared with small molecular CA4 derivatives [37]. However, the solubility of PLG-CA4 is relatively low in water. Alkaline phosphate buffer was used to dissolve PLG-CA4 before adminstration. This is unsuitable for clinical application.

In this study, nanoparticles of poly(L-glutamic acid)-*graft*-methoxy poly(ethylene glycol)/combretastatin A4 sodium salt (CA4-NPs) were prepared to improve the water solubility of PLG-CA4. A combination of CA4-NPs plus sorafenib was tested in subcutaneous and orthotopic H22 hepatic tumor models. The CA4-NPs significantly disrupted established tumor blood vessels, caused extensive tumor necrosis and inhibited tumor growth but increased expression of VEGF-A. Meanwhile, sorafenib significantly downregulated VEGF-A expression and inhibited tumor cell proliferation [29]. This combination has remarkable efficacy for the treatment of HCC (Fig. 1).

2. Experimental section

2.1. Materials

CA4 was bought from Hangzhou Great Forest Biomedical Ltd. (Hangzhou, China). Poly(L-glutamic acid)-*graft*-methoxy poly (ethylene glycol) copolymer (PLG-*g*-mPEG) and PLG-*g*-mPEG grafted CA4 (PLG-CA4) were prepared as described previously with slight modification [37,38]. Nanoparticles of poly(L-glutamic acid)-*graft*-methoxy poly(ethylene glycol)/combretastatin A4 sodium salt (CA4-NPs) were synthesized as described in supporting information. Sorafenib was obtained from Meilun Bio. Tech (Dalian, China). VEGF-A, Ki-67 and CD31 antibodies were purchased from Abcam Company (Cambridge, UK). GAPDH and horseradish peroxidase (HRP)-conjugated goat anti-rabbit IgG secondary antibody were purchased from Abclonal Company (Wuhan, China).

2.2. Cell cultures and animals

Human umbilical vein endothelial cells (HUVECs), purchased from Shanghai Bogoo Biotechnology Co. Ltd., China, were cultured in Dulbecco's modified Eagle's medium (DMEM), containing 10% fetal bovine serum, 100 Units/mL penicillin and 100 Units/mL streptomycin. The cells were incubated at 37 °C in a humidified incubator with an atmosphere of 5% CO_2 atmosphere. Male Kunming mice (body weight 20 ± 2 g, aged 4–5 weeks) were provided by the Laboratory Animal Center of Jilin University (Jilin, China). Male BALB/c mice (body weight 20 ± 2 g, aged 4–6 weeks) were purchased from Vital River (Beijing, China). The whole animal experiments were approved by the Jilin University Animal Care and Use Committee.

2.3. Viability of HUVECs

HUVECs were seeded in 96-well plates with a density of 6000 cells/well and incubated overnight. Subsequently, different drug concentrations of CA4-NPs were added into wells. After incubating for 24, 48 or 72 h, cell viability was measured using MTT assay. The absorbance was read on a Bio-Rad 680 automatic microplate reader at 490 nm. The relative cell viability was calculated by comparing the absorbance of sample wells with control wells without drugs, respectively.

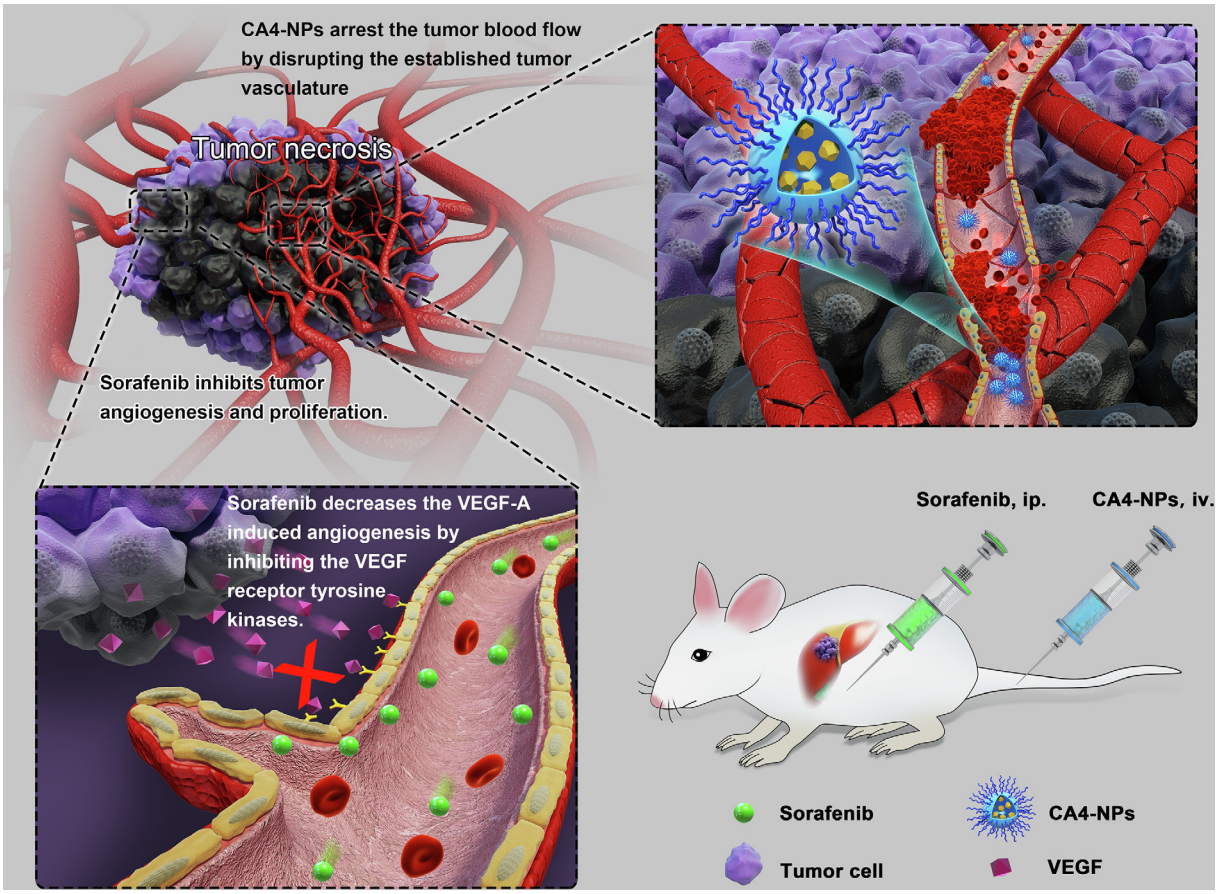

Fig. 1. Cooperative mechanism of CA4-NPs plus sorafenib for systemic therapy of hepatocellular carcinoma. Systemic administration of CA4-NPs leads to the disruption of established tumor blood vessels and extensive tumor necrosis, however, inducing the increase of expression of VEGF-A and angiogenesis. Sorafenib reduces the VEGF-A induced angiogenesis and inhibits tumor proliferation. CA4-NPs plus sorafenib has the potential to completely eradicate the whole tumor of HCC.

2.4. Tube formation assay

To evaluate tube formation, HUVECs cells (4×10^5) were plated on matrigel matrix (BD Biosciences, Palo Alto, CA, USA) in a 96-well plate after gelation of the Matrigel at 37 °C for 40 min. Then cells were treated with vehicle or CA4-NPs (10 μM on CA4 basis) for 12 h before image capture under an inverted optical microscope. Tube disruption assays were conducted in a 96-well plate using HUVECs cells (4×10^5) seeded on Matrigel matrix and allowed to form tubes for 12 h before the addition of drugs. Images were captured at 0 h and 6 h after treatment.

2.5. H22 subcutaneous tumor model

Ivory white ascites were obtained from H22 bearing Kunming mice. H22 ascites was removed via suction and transferred to the abdomen of another mouse three times under aseptic conditions. Cells were washed with normal phosphate-buffered saline (PBS) twice, and diluted with normal PBS into a concentration of 2×10^7 cells/mL. For the subcutaneous tumor model, H22 cells (2×10^6) was injected into the right flank of male BALB/c mice. When tumors grew to approximately 140 mm^3, mice were divided randomly into four groups (n = 7), and treated with PBS, sorafenib, CA4-NPs or sorafenib + CA4-NPs. Treatment was started on day 7 and ended on day 20 post tumor inoculation. CA4-NPs 20 $mg{\cdot}kg^{-1}$ (on the CA4 basis) were given by intravenous (IV) injection *via* tail vein once, and sorafenib 30 $mg{\cdot}kg^{-1}$ was given *via* intraperitoneal (IP) injection each day for 14 days. Tumor volume and mouse body weight were recorded. Tumor volume was calculated as follows: tumor volume (mm^3) = $4\pi ab^2/3$, where a and b represented the longest and shortest radius of the tumor measured by caliper, respectively. Tumor suppression rate was calculated as follows: Tumor suppression rate (TSR%) = $[(Ac - Ax)/Ac] \times 100\%$, where Ac and Ax represented the average volume of tumors in the control and treatment groups, respectively. BALB/c mice were euthanized at day 20 post the tumor inoculation. Serum levels of aspartate aminotransferase (AST), alanine aminotransferase (ALT) and blood urea nitrogen (BUN) were measured using an Automated ChemicalAnalyzer in the First Hospital of Jilin University (Jilin, China).

To identify whether the combination of sorafenib and high-dose CA4-NPs improved anticancer efficacy, subcutaneous H22 bearing mice were administered CA4-NPs 30 $mg{\cdot}kg^{-1}$ (on the CA4 basis), CA4-NPs 35 $mg{\cdot}kg^{-1}$ (on the CA4 basis), sorafenib 30 $mg{\cdot}kg^{-1}$ + CA4-NPs 30 $mg{\cdot}kg^{-1}$ (on the CA4 basis) or sorafenib 30 $mg{\cdot}kg^{-1}$ + CA4-NPs 35 $mg{\cdot}kg^{-1}$ (on the CA4 basis). The method of drug administration was the same as described previously. Tumor volume and mouse body weight were also measured.

2.6. Orthotopic H22 hepatic tumor model

For the *in situ* hepatic tumor model, male BALB/c mice were anesthetized and the liver was exposed under an abdominal midline incision. H22 cells (5×10^5, 25 μL) were injected slowly into the right hepatic lobe and the abdomen was closed with successful establishment of the H22 orthotopic transplantation tumor model. Seven days post tumor inoculation, the mice (n = 6 per group) were divided randomly into the following four treatment groups: (a) PBS, (b) CA4-NPs 30 $mg{\cdot}kg^{-1}$ (on the CA4 basis) IV once on day 7 post tumor inoculation, (c) sorafenib 30 $mg{\cdot}kg^{-1}$ IP once each day for 14 days, (d) sorafenib 30 $mg{\cdot}kg^{-1}$ + CA4-NPs 30 $mg{\cdot}kg^{-1}$

(on the CA4 basis) (the route and frequency of administration were the same as described for the respective drugs in b) and c) above). The tumor weight was recorded at necropsy.

2.7. Histopathological and immunohistochemical analysis

Mice were sacrificed at the end of treatment. Tumors and the major organs (heart, liver, spleen, lung and kidney) from all groups were collected, fixed in 4% paraformaldehyde, embedded in paraffin and sliced at a thickness of 5 μm. The slices were then stained with haematoxylin and eosin (H&E) for histological analysis. Histological images were taken under an optical microscope (IX71, Olympus, Tokyo, Japan). Necrosis areas were semi-quantitatively analyzed with Image J sofware.

Immunohistochemistry was carried out with rabbit monoclonal primary antibodies for Ki-67 and VEGF-A. IHC images of Ki-67 were semi-quantitatively analyzed using Image-Pro Plus software.

2.8. Microvascular density (MVD) evaluation

Subcutaneous H22-bearing BALB/c mice were divided into four groups [PBS, CA4-NPs 20 $mg{\cdot}kg^{-1}$ (on the CA4 basis), sorafenib 30 $mg{\cdot}kg^{-1}$ and the combination group] after the tumor had reached a size of ~140 mm^3. Mice from these four groups were sacrificed at the end of treatment. Tumor-bearing mice from the CA4-NPs 20 $mg{\cdot}kg^{-1}$ (on the CA4 basis) treated group were also sacrificed at varying time points (days 0, 2, 7 and 14) after CA4-NPs injection. Tumors were harvested for CD31 immunohistochemical (IHC) assay. Tumor sections (5 μm-thick) were dewaxed and heated with EDTA (pH = 8) for antigen retrieval·H_2O_2 1.3% was used to block the endogenous peroxidase activity at 37 °C for 15 min. Nonspecific antigens were blocked with normal goat blood serum. Sections were incubated at room temperature with diluted anti-CD31 antibody for 2 h, washed with PBS and incubated with horseradish peroxidase (HRP) conjugated secondary antibodies for 20 min. After being washed with PBS, the slides were exposed to DAB. MVD was examined at ×400 magnification by counting the total number of stained microvessels in three representative areas with the highest neovasculation at a low magnification. The average number of the three areas was the MVD value of the tumor.

2.9. Western blot analysis

Subcutaneous H22 tumor-bearing mice were euthanized after the last drug administration. Tumors were collected and frozen at −80 °C for further use. Total proteins were extracted after being lysed by RIPA lysis buffer. Protein concentration was determined with a BCA assay kit (Thermo Scientific, Rockford, IL, USA). Protein (30 μg) was mixed with 5× loading buffer and boiled for 5 min. Protein samples were loaded into 12% SDS-PAGE gel and transferred onto a PVDF membrane. The membrane was blocked with 5% skimmed milk in 1×TBS containing 0.1% Tween20 and was then incubated waveringly with rabbit primary antibodies, anti-VEGF-A (1:200, Abcam) and anti-GAPDH (1:2000, Abclonal), at 4 °C overnight. The bands were subsequently incubated with HRP-conjugated goat anti-rabbit IgG secondary antibody (1:10000, Abclonal) at room temperature for 1 h. The bands were placed in the chemiluminescent (ECL) working solution and exposed to the Amersham Imager 600 (GE Healthcare, Tokyo, Japan).

2.10. Data analysis

The results are presented as the mean ± standard deviation (SD), and were analyzed using Student's *t*-test when comparing two groups. One-way ANOVA analysis was used when comparing more than two groups. Survival curves were plotted using the Kaplan-Meier method and analyzed with the log-rank test. $^{*}P < 0.05$ was considered statistically significant, whereas $^{**}P < 0.01$ and $^{***}P < 0.001$ were considered highly and extremely significant.

3. Results and discussion

3.1. Synthesis and characterization of CA4-NPs

CA4-NPs were prepared in two steps (Scheme S1). Firstly, PLG-CA4 was prepared by a Yamaguchi reaction; then PLG-CA4 was salined by sodium hydrocarbonate aqueous solution. The detailed preparation process for CA4-NPs was described in supporting information.

The ^{1}H NMR spectrum of CA4-NPs was shown in Figure S1. Typical peaks in the ^{1}H NMR spectrum at δ 6.53 (k + l + m), 6.41 (j) and 6.26 (h + i) ppm should be assigned to the protons of CA4 in the CA4-NPs. Sixty-three percent of glutamic acid moieties was conjugated with CA4. The DLC% of CA4 in the CA4-NPs was 20.8 wt% calculated from the signal intensity ratio of (h + i)/(d + c) in the ^{1}H NMR. HPLC was applied to determine the free CA4 content and the CA4 loading content of CA4-NPs. As shown in Figure S2, a small peak of free CA4 at 3.4 min was present in the spectrum of CA4-NPs, indicating the low content of free CA4 in the CA4-NPs. The DLC% of CA4 in CA4-NPs was 20.5 wt%, and the free CA4 content in CA4-NPs was 2.0 wt%. The size of CA4-NPs was determined by DLS (Figure S3) and the CA4-NPs had a narrow size distribution with a hydrodynamic radius (R_h) of 42.9 ± 10.4 nm. As shown in Figure S4, the TEM image indicated CA4-NPs had a diameter of 56.8 ± 4.8 nm in a dehydrated form. The release of CA4 from CA4-NPs showed a pH-dependent release profile with a release rate of pH 7.4 > pH 6.8 > pH 5.5 (Figure S5). Both CA4-NPs and PLG-CA4 were dissolved in PBS with a concentration of 1.0 $mg{\cdot}kg^{-1}$ (on the CA4 basis). Thirty minutes later, the solution of CA4-NPs was clear and transparent, while the solution of PLG-CA4 is cloudy and opaque (Figure S6). The water solubility of CA4-NPs was obviously higher than PLG-CA4.

3.2. In vitro cytotoxicity assay

MTT assay was conducted to evaluate the cytotoxicity of CA4-NPs on HUVECs. The cell viability data were shown in Figure S7. CA4-NPs displayed time and dose dependent cell inhibition activities on HUVECs. CA4-NPs inhibited the proliferation of HUVECs with an IC50 values of 139.107 μM at 48 h and 0.521 μM at 72 h, respectively. These results demonstrated the antiproliferative activity against human HUVECs of CA4-NPs.

3.3. CA4-NPs inhibit tube formation of endothelial cells

We further evaluated the activity of CA4-NPs on endothelial cells by tube formation in vitro. HUVECs were seeded on Matrigel-coated 96-well plate in the presence or absence of drugs. At 12 h after cells plating, the tube formation activities were investigated by taking photos of HUVECs (Figure S8A). By 12 h, cells in the control group formed tubes, while cells under CA4-NPs (10 μM on CA4 basis) treatment showed almost complete loss of tube structure. Therefore, we demonstrated that CA4-NPs inhibit the formation of new tubes.

To investigate the activity of CA4-NPs on established tube structures, HUVECs were plated on Matrigel and allowed to form tubes for 12 h prior to drug intervention. Figure S8B showed the structure changes of preformed tubes after 6 h exposure to CA4-NPs. Tubes observed 6 h after treatment were still well organized in

the control group, while some tubes were partly disrupted comparing with those before CA4P or CA4-NPs treatment. These results indicated that CA4-NPs was capable of disrupting established tubes.

3.4. Antitumor efficacy and survival time in vivo

The antitumor effects of CA4-NPs monotherapy and the combination of sorafenib + CA4-NPs was evaluated using a mouse H22 subcutaneous tumor model where mice were given PBS, sorafenib 30 mg·kg^{-1}, CA4-NPs 20 mg·kg^{-1} (on the CA4 basis) or sorafenib 30 mg·kg^{-1} + CA4-NPs 20 mg·kg^{-1} (on the CA4 basis) (Fig. 2A). Tumor volumes were monitored each day during treatment to assess the antitumor efficacy of each approach. Both the CA4-NPs and the combination of sorafenib + CA4-NPs showed significant inhibition of H22 tumor growth (Fig. 2B). At day 20 post tumor inoculation, the tumor suppression rate (TSR%) was 81.6% in mice on the combination treatment. This was significantly higher than those in the CA4-NPs (33.0%; $P < 0.001$) and sorafenib (54.7%; $P < 0.001$) monotherapy groups. The greater anticancer efficacy of the combination treatment with sorafenib and CA4-NPs probably resulted from the complementary antivascular mechanisms underlying the therapeutic effect. These results confirmed that sorafenib plus CA4-NPs inhibited H22 tumor growth effectively.

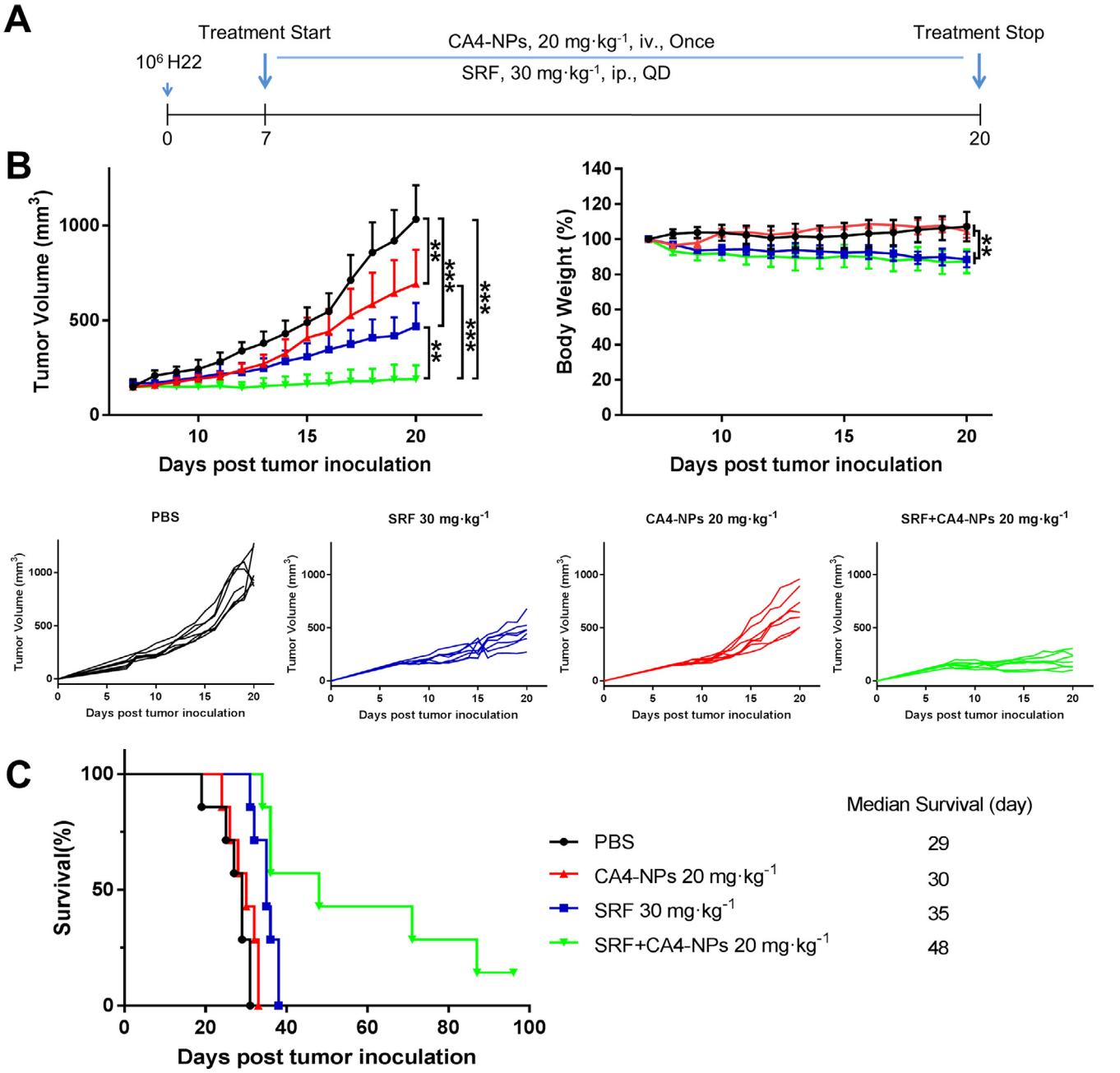

Fig. 2. Combined treatment with sorafenib and CA4-NPs had better antitumor efficacy than CA4-NPs or sorafenib in a subcutaneous H22 tumor model. (A) Treatment scheme. (B) Tumor volumes and body weight change rates of H22 tumor-bearing mice after being administrated with PBS, CA4-NPs 20 mg·kg^{-1} (on the CA4 basis), sorafenib 30 mg·kg^{-1} or sorafenib 30 mg·kg^{-1} + CA4-NPs 20 mg·kg^{-1} (on the CA4 basis). Average and individual H22 tumor growth curves are illustrated. (C) Combinined therapy of sorafenib 30 mg·kg^{-1} and CA4-NPs 20 mg·kg^{-1} (on the CA4 basis) prolonged survival of subcutaneous H22 bearing mice. Kaplan-Meier survival analysis for subcutaneous H22 bearing mice in the four treatment groups noted above (log-rank test, n = 7). Mice were killed once their tumor volume was >2000 mm^3. Data are shown as mean ± SD ($^{**}P < 0.01$, $^{***}P < 0.001$).

Mouse body weight changes were monitored as a surrogate for the adverse effects of the drugs. As depicted in Fig. 2B, mice receiving CA4-NPs showed about 2.4% body weight loss by the second day of treatment compared with baseline, and this soon returned back to the initial body weight. Mice treated with combination therapy had <12% body weight loss, which was similar to the 11% loss with sorafenib monotherapy at day 20 post tumor inoculation. None of the mice treated with CA4-NPs or sorafenib died during the entire treatment process. H&E staining did not identify any obvious major organ tissue injury at the end of treatment (Figure S9). These results demonstrated a tolerable side effect profile of both sorafenib and CA4-NPs, administered separately or in combination.

In addition to tumor volume, the survival rate of treated mice was determined to evaluate the therapeutic effect of the various treatments. As shown in Fig. 2C, the median survival time of the sorafenib group and the combination treatment group was 35 and 48 days, respectively. The combination treatment yielded a significant survival advantage compared with PBS (median survival time was 29 days). However, CA4-NPs alone achieved a median survival time of 30 days, which was not prolonged compared with the PBS group. Although CA4-NPs monotherapy did not extend survival time in mice, combination treatment increased survival in H22-bearing mice compared with sorafenib alone. The reason of death might be owing to the tumor burden caused by subcutaneous tumor and large amount of ascites. In addition, mice were killed for ethic reasons once their tumor volume reached a size of 2000 mm^3. These data confirmed that the combined application of sorafenib and CA4-NPs could improve the survival time of H22-bearing mice.

AST, ALT and BUN levels were measured to assess liver and kidney function in treated mice. As depicted in Fig. 3, serum AST levels were increased in H22-bearing mice in the PBS group compared with healthy BALB/c mice (normal), which might be ascribed to the acute liver damage caused by tumor burden. Serum AST levels were decreased significantly in the three treatment groups (CA4-NPs, sorafenib and sorafenib + CA4-NPs) compared with the PBS group after 14 days of drug therapy. It might be owing to the effective therapeutic efficacy of CA4-NPs and sorafenib that can reduce tumor burden and therefore improve the state of livers [39]. There was no statistically significant difference in serum ALT and BUN levels between all the groups. The liver and kidney function analyses, especially the AST levels, indicated that both CA4-NPs and sorafenib protected liver function and had no influence on kidney condition in H22 tumor-bearing mice. Routine blood tests, including white blood cell (WBC), red blood cells (RBC), hemoglobin (HGB), hematocrit (HCT) and other hematological parameters, were also examined on healthy Kunming mice to further evaluate the biocompatibility of CA4-NPs and the combination groups. As shown in **Figure S10,** levels of hematological parameters in the different treatment groups were within normal range, which demonstrated that the combination of CA4-NPs and sorafenib had no myelosuppression effect or hematological toxicity. In addition to these parameters, the metabolism of CA4-NPs will be studied in detail in the future.

3.5. Histopathological and Ki-67 immunohistochemical analysis

H&E staining was performed to verify antitumor efficacy comprehensively. As depicted in Fig. 4A, significant pathological differences were shown, with nuclei in necrotic areas appearing pyknotic, cataclastic and even absent. Semi-quantitative analysis of necrotic areas was performed. As shown in Fig. 4B, the necrotic area in the CA4-NPs 20 $mg{\cdot}kg^{-1}$ (on the CA4 basis), sorafenib 30 $mg{\cdot}kg^{-1}$ and the combination treatment groups were 46.8 ± 3.3%, 44.6 ± 0.5% and 86.9 ± 5.6%, respectively. In the combination treatment group, the vast majority of tumor cells were eradicated and, in some cases, the entire tumor was disappeared. These results were in accordance with the changes in tumor volume *in vivo* and confirmed the improved tumor inhibition ability of sorafenib + CA4-NPs over either agent administered alone.

We further examined the expression of Ki-67, a marker of cell proliferation [40–42]. Fig. 4A shows representative images of Ki-67 IHC staining. Semi-quantitative analysis of Ki-67 (Fig. 4C) indicated that the highest Ki-67 expression was in the PBS group of H22 tumor-bearing mice, while the lowest Ki-67 expression was in the combination group. These results indicated that H22 cells grew the fastest in the PBS group, and grew the slowest in the combination group. These data further confirmed that the combined treatment approach restrained tumor cell proliferation in H22 tumor-bearing mice effectively.

3.6. CD31 tumor expression

CD31 is a marker of vascular endothelial cells related to the density of tumor vasculature. Here, tumor vessel density was evaluated by staining CD31 for IHC and counting the number of stained microvessels. To investigate tumor microvascular changes after a single dose of CA4-NPs, we analyzed CD31 expression in tumors on days 0, 2, 7 and 14 after CA4-NPs treatment. The CD31 staining images of mice in CA4-NPs group were taken in the surrounding area of the tumor. The mean (±SD) MVD of CD31 positive sections

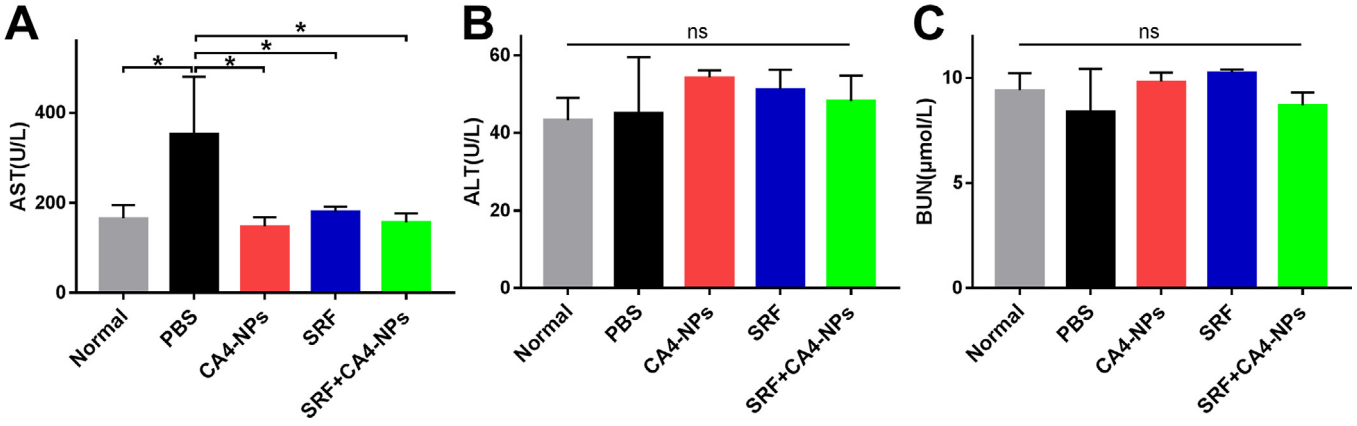

Fig. 3. Function assessment in H22 subcutaneous tumor model. (A-C) Serum AST, ALT and BUN levels were monitored at day 14 on treatment with PBS, sorafenib 30 $mg{\cdot}kg^{-1}$, CA4-NPs 20 $mg{\cdot}kg^{-1}$ (on the CA4 basis) or sorafenib 30 $mg{\cdot}kg^{-1}$ + CA4-NPs 20 $mg{\cdot}kg^{-1}$ (on the CA4 basis). Data are shown as mean ± SD (*P < 0.05). "Normal" mice represent healthy BALB/c mice.

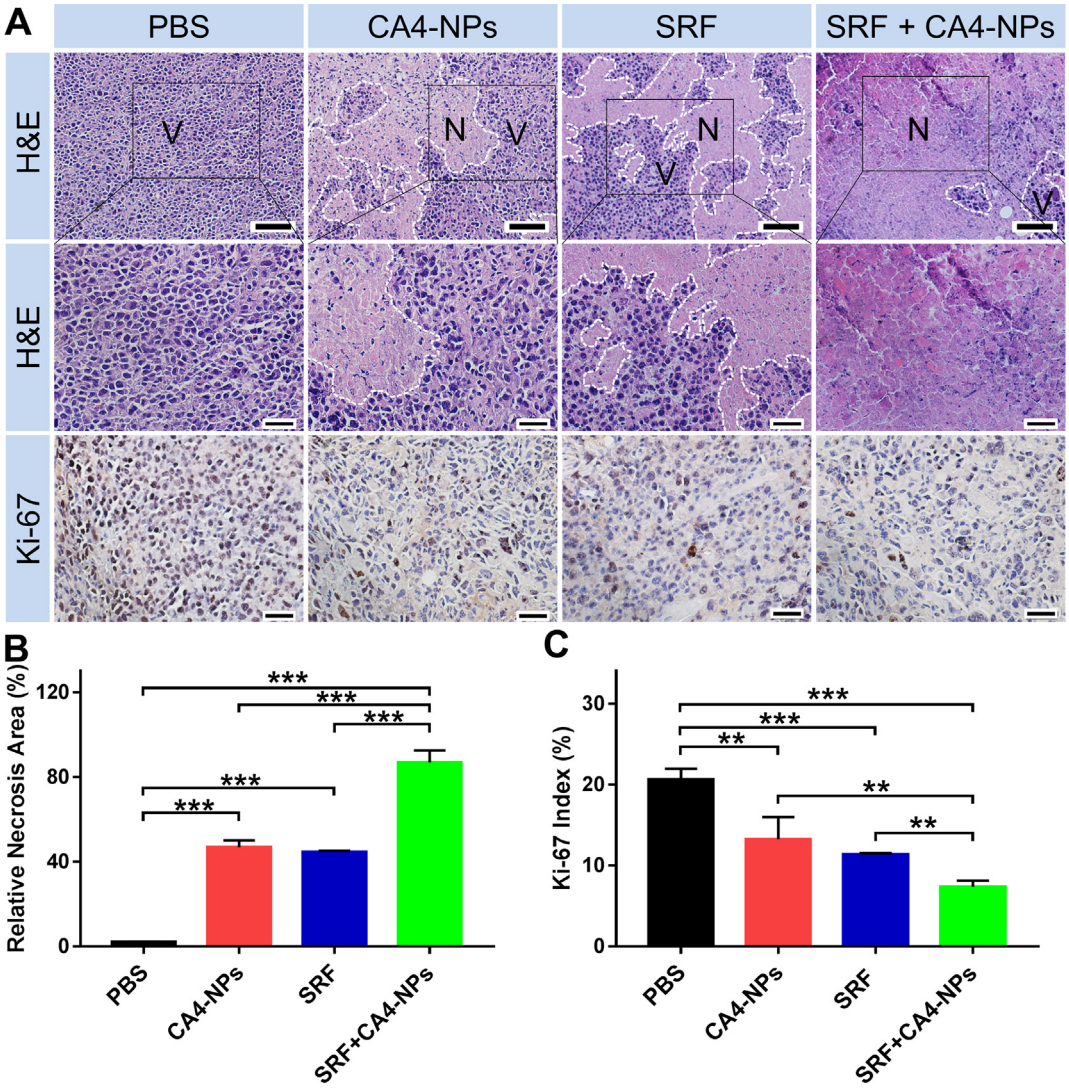

Fig. 4. H&E and Ki-67 analyses of H22 tumor sections at day 14 after treatment with PBS, CA4-NPs 20 mg·kg^{-1} (on the CA4 basis), sorafenib 30 mg·kg^{-1} or sorafenib 30 mg·kg^{-1} + CA4-NPs 20 mg·kg^{-1} (on the CA4 basis). (A) H&E images were taken at × 100 magnification (up) and × 400 magnification (down). Ki-67 were taken at × 400 magnification. (B) Semi-quantitative analysis of relative necrotic area in tumors. (C) Semi-quantitative analysis of Ki-67 expression. The scale bars of H&E represent 50 μm (up) and 20 μm (down). The scale bars of Ki-67 represent 20 μm. Data are shown as mean ± SD ($^{*}P < 0.05$, $^{***}P < 0.001$). N, necrotic region of tumors; V, viable region of tumors.

was remarkably lower on day 2 (22.7 ± 1.5) and day 7 (23.7 ± 1.5) compared with day 0 (41.3 ± 3.8). However, MVD was apparently higher on day 14 (73.0 ± 4.6), which was almost two times that on day 0 (Fig. 5A and B). These results demonstrated that CA4-NPs disrupted established tumor vasculature and maintained tumor vessel density at a relatively low level for at least 7 days. However, re-establishment of tumor vasculature occurred two weeks after the first drug injection indicating induced angiogenesis by CA4-NPs.

In addition to this, we evaluated CD31 expression in the four treatment groups noted above on day 14 after treatment initiation. As shown in Fig. 5C and D, the sorafenib + CA4-NPs group showed the lowest mean MVD (7.3 ± 0.6), compared with the PBS (14.3 ± 0.6), sorafenib (10.0 ± 1.0) and CA4-NPs (73.0 ± 4.6) groups. The possible mechanism for the low MVD with the combination of sorafenib and CA4-NPs is that, CA4-NPs significantly disrupt established tumor vasculature and suppressed tumor growth, while continuous administration of sorafenib inhibited revascularization and regrowth of the treated tumor. These data demonstrated that treatment with sorafenib plus CA4-NPs reduced angiogenesis of the tumor significantly.

3.7. VEGF-A tumor expression

We next measured VEGF-A expression by IHC and western blot in each group to further investigate the tumor inhibition mechanism of sorafenib + CA4-NPs in the subcutaneous H22-bearing mouse model. Semi-quantitative analyses of VEGF-A by western blot were also performed. As shown in Fig. 6, the order of the extent of VEGF-A expression was calculated as follows: CA4-NPs > PBS > sorafenib + CA4-NPs > sorafenib. Expression of VEGF-A was significantly less after administration of sorafenib with CA4-NPs compared with CA4-NPs alone. The IHC results for VEGF-A expression were consistent with the western blot analysis. Upregulation of angiogenic factors, such as VEGF-A, induced by VDAs can promote proliferation of neovasculature and tumor regrowth in the tumor periphery [43,44]. Inhibitors of VEGFR-associated tyrosine kinase are promising agents to abolish the angiogenic activity of VEGF-A. Sorafenib, a VEGFR tyrosine kinase inhibitor, is an antiangiogenic agent that can disturb re-establishment of tumor vasculature and inhibit tumor cell proliferation [45]. These data indicated that combined treatment with sorafenib + CA4-NPs significantly decreased VEGF-A expression compared to CA4-NPs

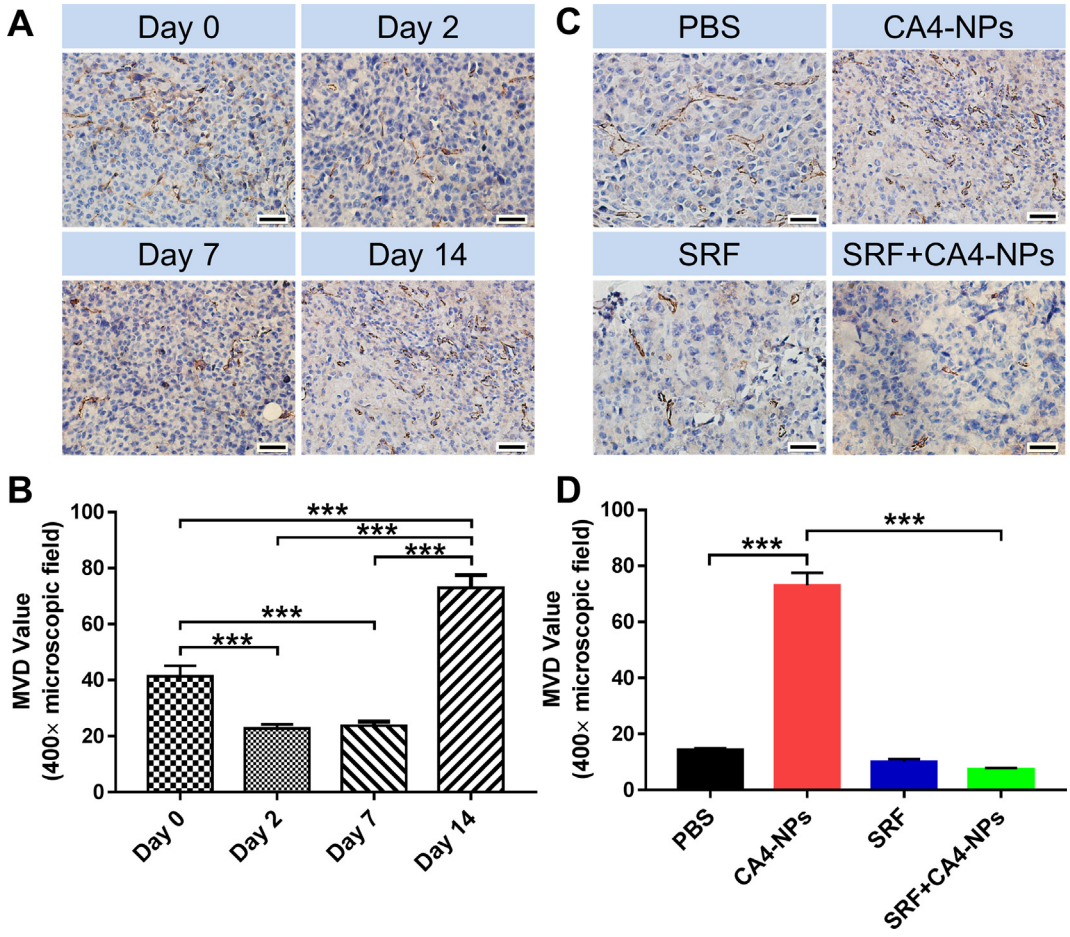

Fig. 5. Immunohistochemical reactivity for blood vessel endothelial cell marker CD31 in subcutaneous H22 bearing mice. (A) CD31 immunohistochemical staining of tumor sections after treatment with CA4-NPs 20 mg·kg^{-1} (on the CA4 basis) at day 0, 2, 7 and 14. (B) IHC staining for CD31 in tumor tissues at day 14 post treatment with PBS, CA4-NPs 20 mg·kg^{-1} (on the CA4 basis), sorafenib 30 mg·kg^{-1} or sorafenib 30 mg·kg^{-1} plus CA4-NPs 20 mg·kg^{-1} (on the CA4 basis). (C) Mean microvessel density of CD31 in (A). (D) Mean microvessel density of CD31 in (B). All images were taken at × 400 magnification. Scale bars represent 20 μm. Data are shown as mean ± SD ($^{*}P < 0.05$, $^{**}P < 0.01$ and $^{***}P < 0.001$).

monotherapy, and alleviated the VEGF-mediated angiogenesis process.

3.8. Combination therapy with high-dose CA4-NPs

To identify whether the combination of sorafenib with higher doses of CA4-NPs could improve anticancer efficacy, subcutaneous H22 bearing mice were given PBS, CA4-NPs 30 mg·kg^{-1} (on the CA4 basis), CA4-NPs 35 mg·kg^{-1} (on the CA4 basis), sorafenib 30 mg·kg^{-1} + CA4-NPs 30 mg·kg^{-1} (on the CA4 basis) or sorafenib 30 mg·kg^{-1} + CA4-NPs 35 mg·kg^{-1} (on the CA4 basis) (Fig. 7A). As observed in the subcutaneous H22 tumors, all four treatments reduced tumor burden efficiently (Fig. 7B). The anticancer efficacy was improved as the dose of CA4-NPs increased. On day 20 post tumor inoculation, there were 3 out of 7 mice without visible tumor in the group treated with CA4-NPs 35 mg·kg^{-1} (on the CA4 basis), however, tumor recurrence happened in two mice later on (Data not shown). On day 20, the TSR% of mice receiving CA4-NPs 35 mg·kg^{-1} (on the CA4 basis) was 95.3%, which was significantly higher than that of mice receiving CA4-NPs 30 mg·kg^{-1} (on the CA4 basis, 51.7%). This dramatic difference in the antitumor efficacy between treatments of CA4-NPs 30 mg·kg^{-1} (on the CA4 basis) and CA4-NPs 35 mg·kg^{-1} (on the CA4 basis) should be attributed to the long time interval (14 days) between CA4-NPs administration and tumor volume measurement. As for the combination therapy groups, the TSR% was 92.9% for sorafenib 30 mg·kg^{-1} + CA4-NPs 30 mg·kg^{-1} (on the CA4 basis) and 93.7% for sorafenib 30 mg·kg^{-1} + CA4-NPs 35 mg·kg^{-1} (on the CA4 basis). CA4-NPs monotherapy was equivalent or more effective than sorafenib (54.7%), especially at a CA4-NPs dose of 35 mg·kg^{-1} (on the CA4 basis). With respect to combination therapy, tumor volumes were lower than in the CA4-NPs or sorafenib monotherapy groups when CA4-NPs was given at a CA4 dose of 30 mg·kg^{-1}. However, there was no significant difference in tumor volume between CA4-NPs 35 mg·kg^{-1} (on the CA4 basis) and its combination with sorafenib 30 mg·kg^{-1} as a result of the excellent efficacy of CA4-NPs at the high dose. These data further confirmed the favorable anticancer efficacy of combined sorafenib and CA4-NPs.

In terms of drug toxicity, CA4-NPs doses of 30 and 35 mg·kg^{-1} (on the CA4 basis) resulted in a greater body weight loss of 7.4% and 10.1%, respectively, by day 2 after the first CA4-NPs treatment compared with CA4-NPs 20 mg·kg^{-1} (on the CA4 basis, 2.4%). However, body weight returned to baseline one week later (Fig. 7B). The rate of body weight change in the combination therapy groups with high doses of CA4-NPs were almost the same as with the CA4-NPs 20 mg·kg^{-1} (on the CA4 basis) combined group. These data demonstrated the tolerable toxicity of combined sorafenib and CA4-NPs in relatively high doses.

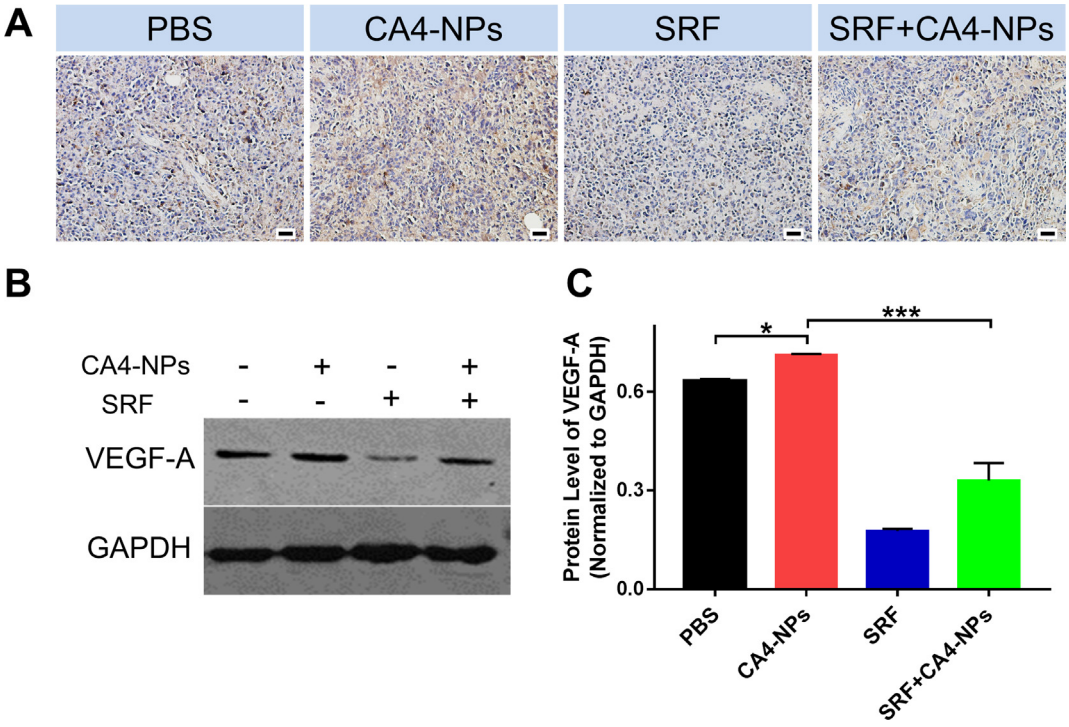

Fig. 6. VEGF-A expression in H22-bearing mice in each group. (A) VEGF-A immunohistochemical staining at day 14 on treatment with PBS, CA4-NPs 20 mg·kg^{-1} (on the CA4 basis), sorafenib 30 mg·kg^{-1} or sorafenib 30 mg·kg^{-1} plus CA4-NPs 20 mg·kg^{-1} (on the CA4 basis). (B) Detection of VEGF-A by western blot in each group on day 14 after the first drug injection. (C) Semi-quantitative analysis of VEGF-A expression by western blot. Scale bar = 20 μm. Data are shown as mean ± SD ($^{*}P < 0.05$, $^{**}P < 0.01$, $^{***}P < 0.001$).

On account of the encouraging *in vivo* TSR% results, we further identified the effects on survival time of CA4-NPs 30 mg·kg^{-1} (on the CA4 basis), CA4-NPs 35 mg·kg^{-1} (on the CA4 basis), sorafenib 30 mg·kg^{-1} + CA4-NPs 30 mg·kg^{-1} (on the CA4 basis) or sorafenib 30 mg·kg^{-1} + CA4-NPs 35 mg·kg^{-1} (on the CA4 basis). As depicted in Fig. 7C, the median survival time of mice receiving CA4-NPs 30 mg·kg^{-1} (on the CA4 basis) was 30 days, and for 35 mg·kg^{-1} (on the CA4 basis) was 46 days. The combination treatment significantly prolonged survival of H22 tumor-bearing mice compared with the single drug treatment groups. The median survival time of mice in the combination groups was more than 96 days. These findings indicated that mice obtained survival benefits from combination therapy in the long run. At the end of the observation period, all mice died in the CA4-NPs 30 mg·kg^{-1} group. One out of seven mice was alive without residual tumor in the CA4-NPs 35 mg·kg^{-1} group (on the CA4 basis). In contrast, five out of seven treated mice were alive without residual tumor in the combination treatments with CA4 doses of 30 or 35 mg·kg^{-1} (Fig. 7C). Tumor characteristics such as tumor volume, weight change rate and survival data of all the subcutaneous H22-bearing mice treatment groups are shown in Figure S11. The combined therapy of CA4-NPs and sorafenib present effctive anticancer efficacy. In order to investigate whether improved anticancer efficacy might be achieved by co-loading of sorafenib and CA4 or not, we will try to co-load these two drugs into one nanoparticle in the future. These confirmed that combined treatment with sorafenib and CA4-NPs prolonged survival time of the H22-tumor bearing mice, with sorafenib 30 mg·kg^{-1} + CA4-NPs 30 mg·kg^{-1} (on the CA4 basis) the optimal formulation to treat tumors.

3.9. Therapeutic efficacy in the orthotopic H22 hepatic tumor model in vivo

Orthotopic implantation of hepatoma-bearing mice is representative of spontaneous liver cancer and is recommended for study of HCC [39]. Herein, H&E tumor staining was performed to verify the antitumor efficacy of combined sorafenib 30 mg·kg^{-1} + CA4-NPs 30 mg·kg^{-1} (on the CA4 basis) therapy in the orthotopic H22 hepatic tumor model. Tumor weight was recorded after excision from the body 14 days after treatment initiation. Fig. 8A and B shows the appearance of liver cancer and H&E staining in the different groups, with semi-quantitative analysis presented in Fig. 8C. During the therapeutic process, different degrees of necrosis were observed in the CA4-NPs 30 mg·kg^{-1} (on the CA4 basis), sorafenib 30 mg·kg^{-1} and their combination therapy groups. Further, a large quantity of fragmented nuclei and massive necrosis occurred after co-administration of sorafenib and CA4-NPs. Both the CA4-NPs (50.5%) and sorafenib (50.7%) alone groups showed significantly increased necrotic areas compared with the PBS group (10.1%). Noteworthy, the largest necrotic area appeared in the combined therapy group (78.7%). In regard to excised tumor weight, the sorafenib + CA4-NPs group had the lightest tumor weight of all the groups, being much lower than the PBS group and significantly less than the CA4-NPs or sorafenib groups (Fig. 8D). CA4-NPs monotherapy, sorafenib monotherapy and combined sorafenib plus CA4-NPs therapy were effective in slowing tumor growth compared with the PBS group. These data agreed with those of the H22 subcutaneous tumor model, and further verified the high antitumor effect of the combination of sorafenib plus CA4-NPs.

CD31 IHC staining was evaluated to investigate the tumor vessels in orthotopic H22 hepatic tumor model. As shown in Figure S12A, tumor blood vessels has been established at day 7 after tumor inoculation. We also evaluated the vessels of tumors after being treated with PBS or co-administration of sorafenib and CA4-NPs. CD31 was significantly reduced in the combined treatment group compared with the PBS group at the end of treatment (Figure S12B and C). These data demonstrated that co-administration of CA4-NPs and sorafenib could also reduce angiogenesis of orthotopic H22 hepatic tumor models.

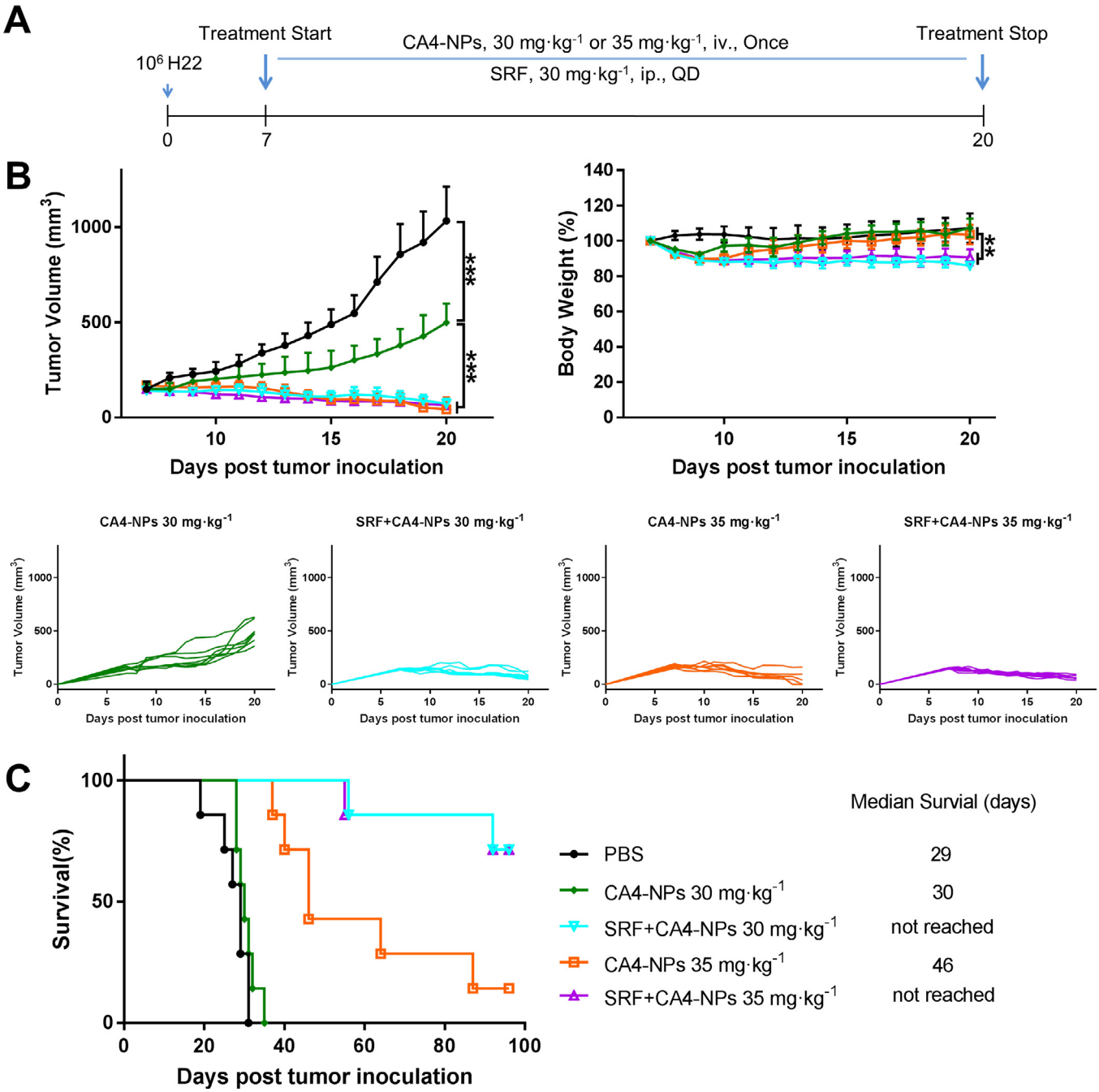

Fig. 7. Anticancer efficacy of high-dose CA4-NPs and combined therapies in subcutaneous H22 bearing mice. (A) Treatment scheme. (B) Tumor volumes and body weight change rates of mice treated with PBS, CA4-NPs 30 mg·kg^{-1} (on the CA4 basis), sorafenib 30 mg·kg^{-1} + CA4-NPs 30 mg·kg^{-1} (on the CA4 basis), CA4-NPs 35 mg·kg^{-1} (on the CA4 basis) or sorafenib 30 mg·kg^{-1} + CA4-NPs 35 mg·kg^{-1} (on the CA4 basis). (C) Kaplan-Meier survival analysis for subcutaneous H22 bearing mice (log-rank test, n = 7). Mice were killed once their tumor volume was >2000 mm^3. Data are shown as mean ± SD ($^{**}P < 0.01$, $^{***}P < 0.001$).

4. Conclusion

In this study, a combination of sorafenib plus nanoparticles of poly(L-glutamic acid)-*graft*-methoxy poly(ethylene glycol)/combretastatin A4 sodium salt (CA4-NPs) was developed for systemic treatment of HCC. The CA4-NPs could significantly disrupt established tumor blood vessels and cause extensive tumor necrosis, however, meanwhile inducing increased expression of VEGF-A in the treated tumors. The sorafenib significantly downregulated VEGF-A expression and alleviated the VEGF-mediated angiogenesis process. The combination of sorafenib 30 mg·kg^{-1} + CA4-NPs 30 mg·kg^{-1} (on the CA4 basis) showed an over 90% tumor suppression rate in a hepatic H22 subcutaneous tumor model with low systemic toxicity. Five out of seven treated mice survived in tumor-free state for 96 days. These findings indicated that the two-pronged attack of sorafenib with a tumor blood-flow reducer, CA4-NPs, was a promising therapeutic approach for HCC treatment.

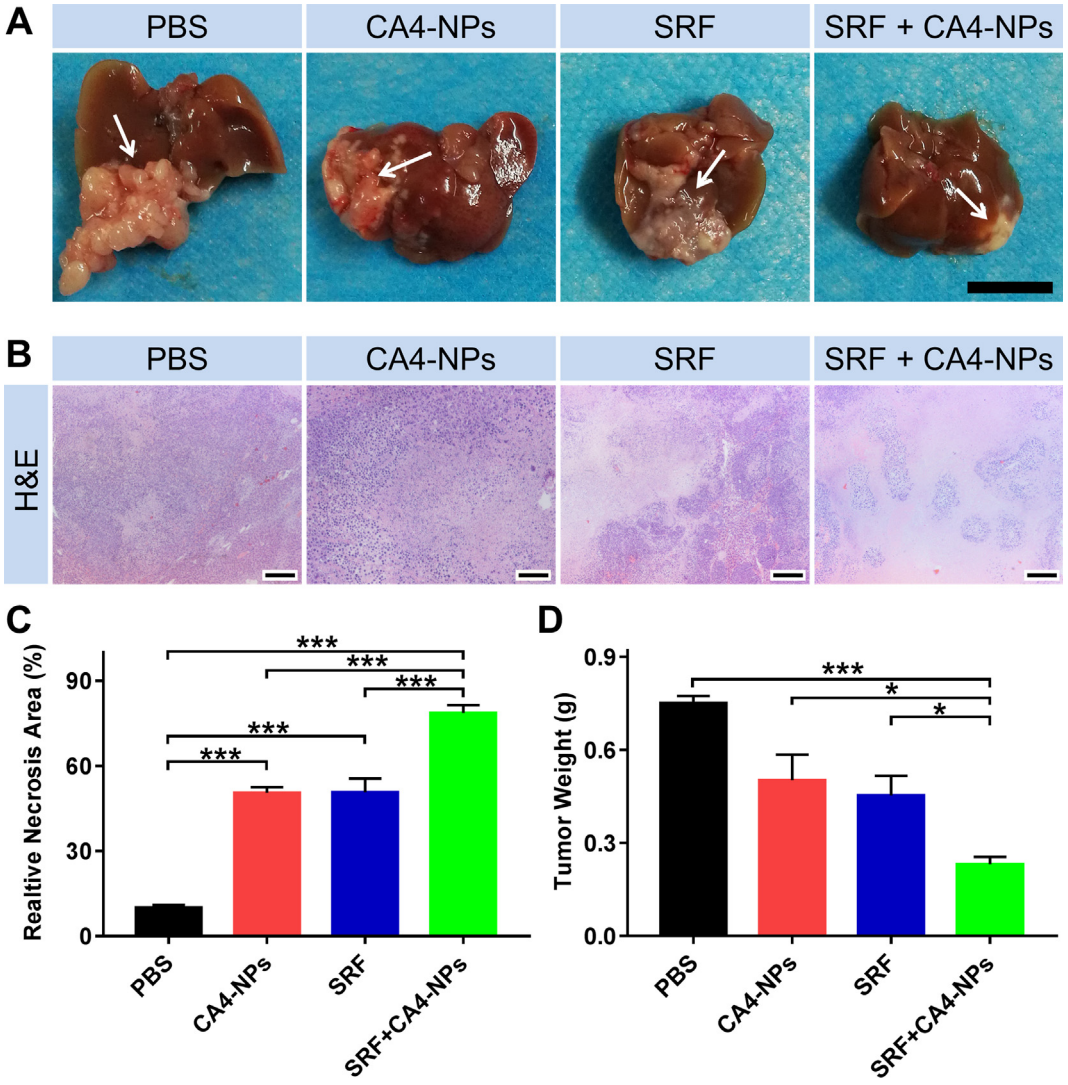

Fig. 8. Sorafenib plus CA4-NPs was effective against orthotopic H22 xenograft mice model. (A) Photographs of liver tumors at day 14 post treatment with PBS, CA4-NPs 30 mg·kg^{-1} (on the CA4 basis), sorafenib 30 mg·kg^{-1} or sorafenib 30 mg·kg^{-1} plus CA4-NPs 30 mg·kg^{-1} (on the CA4 basis). (B) H&E images. (C) Percent of relative necrostic areas. (D) The tumor weight was monitored. The scale bars represent (tumor) 1 cm and (H&E) 200 μm, respectively. Data are shown as mean ± SD ($^{*}P < 0.05$, $^{***}P < 0.001$).

Competing interests

The authors have declared that no competing interest exists.

Acknowledgements

This work was financially supported by Ministry of Science and Technology of China (Project 2016YFC1100701 and 2018ZX09711003-012), National Natural Science Foundation of China (Projects 51673189, 51873206, 51673185 and 51829302), the Program of Scientific Development of Jilin Province (No. 20170101100JC and 20170623009TC), Development and Reform Commission of Jilin Province (No. 3J117B963428) and Science and Technology Service Network Initiative (Project KFJ-SW-STS-166).

Appendix A. Supplementary data

Supplementary data to this article can be found online at https://doi.org/10.1016/j.actbio.2019.05.028.

References

[1] M.E. Nelson, S. Lahiri, J.D. Chow, F.L. Byrne, S.R. Hargett, D.S. Breen, E.M. Olzomer, L.E. Wu, G.J. Cooney, N. Turner, D.E. James, J.K. Slack-Davis, C. Lackner, S.H. Caldwell, K.L. Hoehn, Inhibition of hepatic lipogenesis enhances liver tumorigenesis by increasing antioxidant defence and promoting cell survival, Nat. Commun. 8 (2017) 14689.
[2] H. Zeng, R. Zheng, Y. Guo, S. Zhang, X. Zou, N. Wang, L. Zhang, J. Tang, J. Chen, K. Wei, S. Huang, J. Wang, L. Yu, D. Zhao, G. Song, J. Chen, Y. Shen, X. Yang, X. Gu, F. Jin, Q. Li, Y. Li, H. Ge, F. Zhu, J. Dong, G. Guo, M. Wu, L. Du, X. Sun, Y. He, M.P. Coleman, P. Baade, W. Chen, X.Q. Yu, Cancer survival in China, 2003–2005: a population-based study, Int. J. Cancer 136 (8) (2015) 1921–1930.
[3] A. Forner, M. Reig, J. Bruix, Hepatocellular carcinoma, Lancet (London, England) 391 (10127) (2018) 1301–1314.
[4] H. Yan, J. Chen, Y. Li, Y. Bai, Y. Wu, Z. Sheng, L. Song, C. Liu, H. Zhang, Ultrasmall hybrid protein-copper sulfide nanoparticles for targeted photoacoustic imaging of orthotopic hepatocellular carcinoma with a high signal-to-noise ratio, Biomater. Sci. 7 (1) (2018) 92–103.
[5] F. Shi, S. Lian, P. Wu, L. Shen, Transarterial chemoembolization with or without microwave ablation in the treatment of intermediate (BCLC B) hepatocellular carcinoma, J. Clin. Oncol. 35 (15_suppl) (2017). e15635 e15635.
[6] M. Kudo, K. Imanaka, N. Chida, K. Nakachi, W.Y. Tak, T. Takayama, J.H. Yoon, T. Hori, H. Kumada, N. Hayashi, S. Kaneko, H. Tsubouchi, D.J. Suh, J. Furuse, T. Okusaka, K. Tanaka, O. Matsui, M. Wada, I. Yamaguchi, T. Ohya, G. Meinhardt, K. Okita, Phase III study of sorafenib after transarterial chemoembolisation in Japanese and Korean patients with unresectable hepatocellular carcinoma, Eur. J. Cancer (Oxford, England: 1990) 47 (14) (2011) 2117–2127.

[7] S.L. Chan, W. Yeo, F. Mo, A.W.H. Chan, J. Koh, L. Li, E.P. Hui, C.C.N. Chong, P.B.S. Lai, T.S.K. Mok, S.C.H. Yu, A phase 2 study of the efficacy and biomarker on the combination of transarterial chemoembolization and axitinib in the treatment of inoperable hepatocellular carcinoma, Cancer 123 (20) (2017) 3977–3985.
[8] D. Mao, M. Zhu, X. Zhang, R. Ma, X. Yang, T. Ke, L. Wang, Z. Li, D. Kong, C. Li, A macroporous heparin-releasing silk fibroin scaffold improves islet transplantation outcome by promoting islet revascularisation and survival, Acta Biomater. 59 (2017) 210–220.
[9] M.A. Wilson, F. Zhao, R. Letrero, K. D'Andrea, D.L. Rimm, J.M. Kirkwood, H.M. Kluger, S.J. Lee, L.M. Schuchter, K.T. Flaherty, K.L. Nathanson, Correlation of somatic mutations and clinical outcome in melanoma patients treated with Carboplatin, Paclitaxel, and sorafenib, Clin. Cancer Res.: An Off. J. Am. Assoc. Cancer Res. 20 (12) (2014) 3328–3337.
[10] A.L. Cheng, S. Thongprasert, H.Y. Lim, W. Sukeepaisarnjaroen, T.S. Yang, C.C. Wu, Y. Chao, S.L. Chan, M. Kudo, M. Ikeda, Y.K. Kang, H. Pan, K. Numata, G. Han, B. Balsara, Y. Zhang, A.M. Rodriguez, Y. Zhang, Y. Wang, R.T. Poon, Randomized,, open-label phase 2 study comparing frontline dovitinib versus sorafenib in patients with advanced hepatocellular carcinoma, Hepatology (Baltimore, MD) 64 (3) (2016) 774–784.
[11] R. Pinyol, R. Montal, L. Bassaganyas, D. Sia, T. Takayama, G.Y. Chau, V. Mazzaferro, S. Roayaie, H.C. Lee, N. Kokudo, Z. Zhang, S. Torrecilla, A. Moeini, L. Rodriguez-Carunchio, E. Gane, C. Verslype, A.E. Croitoru, U. Cillo, M. de la Mata, L. Lupo, S. Strasser, J.W. Park, J. Camps, M. Sole, S.N. Thung, A. Villanueva, C. Pena, G. Meinhardt, J. Bruix, J.M. Llovet, Molecular predictors of prevention of recurrence in HCC with sorafenib as adjuvant treatment and prognostic factors in the phase 3 STORM trial, Gut (2018).
[12] M. Kudo, K. Ueshima, M. Ikeda, T. Torimura, N. Tanabe, H. Aikata, N. Izumi, T. Yamasaki, S. Nojiri, K. Hino, H. Tsumura, T. Kuzuya, N. Isoda, K. Yasui, K. Yoshimura, T. Okusaka, J. Furuse, N. Kokudo, K. Okita, Y. Arai, F.t.T.T. Group, Randomized open label, multicenter, phase II trial comparing transarterial chemoembolization (TACE) plus sorafenib with TACE alone in patients with hepatocellular carcinoma (HCC): TACTICS Trial, J. Clin. Oncol. 36 (4_suppl) (2018). 206-206.
[13] A. Forner, M. Gilabert, J. Bruix, J.L. Raoul, Treatment of intermediate-stage hepatocellular carcinoma, nature reviews, Clin. Oncol. 11 (9) (2014) 525–535.
[14] Y. Chao, Y.H. Chung, G. Han, J.H. Yoon, J. Yang, J. Wang, G.L. Shao, B.I. Kim, T.Y. Lee, The combination of transcatheter arterial chemoembolization and sorafenib is well tolerated and effective in Asian patients with hepatocellular carcinoma: final results of the START trial, Int. J. Cancer 136 (6) (2015) 1458–1467.
[15] X. Lei, M. Chen, M. Huang, X. Li, C. Shi, D. Zhang, L. Luo, Y. Zhang, N. Ma, H. Chen, H. Liang, W. Ye, D. Zhang, Desacetylvinblastine monohydrazide disrupts tumor vessels by promoting VE-cadherin internalization, Theranostics 8 (2) (2018) 384–398.
[16] M. Chen, X. Lei, C. Shi, M. Huang, X. Li, B. Wu, Z. Li, W. Han, B. Du, J. Hu, Q. Nie, W. Mai, N. Ma, N. Xu, X. Zhang, C. Fan, A. Hong, M. Xia, L. Luo, A. Ma, H. Li, Q. Yu, H. Chen, D. Zhang, W. Ye, Pericyte-targeting prodrug overcomes tumor resistance to vascular disrupting agents, J. Clin. Investig. 127 (10) (2017) 3689–3701.
[17] Y. Shaked, A. Ciarrocchi, M. Franco, C.R. Lee, S. Man, A.M. Cheung, D.J. Hicklin, D. Chaplin, F.S. Foster, R. Benezra, R.S. Kerbel, Therapy-induced acute recruitment of circulating endothelial progenitor cells to tumors, Science (New York, N.Y.) 313 (2006) 1785–1787.
[18] D.M. Chase, D.J. Chaplin, B.J. Monk, The development and use of vascular targeted therapy in ovarian cancer, Gynecol. Oncol. 145 (2) (2017) 393–406.
[19] J.Y. Blay, Z. Papai, A.W. Tolcher, A. Italiano, D. Cupissol, A. Lopez-Pousa, S.P. Chawla, E. Bompas, N. Babovic, N. Penel, N. Isambert, A.P. Staddon, E. Saada-Bouzid, A. Santoro, F.A. Franke, P. Cohen, S. Le-Guennec, G.D. Demetri, Ombrabulin plus cisplatin versus placebo plus cisplatin in patients with advanced soft-tissue sarcomas after failure of anthracycline and ifosfamide chemotherapy: a randomised, double-blind, placebo-controlled, phase 3 trial, Lancet Oncol. 16 (5) (2015) 531–540.
[20] J.A. Sosa, R. Elisei, B. Jarzab, J. Balkissoon, S.P. Lu, C. Bal, S. Marur, A. Gramza, R. B. Yosef, B. Gitlitz, B.R. Haugen, F. Ondrey, C. Lu, S.M. Karandikar, F. Khuri, L. Licitra, S.C. Remick, Randomized safety and efficacy study of fosbretabulin with paclitaxel/carboplatin against anaplastic thyroid carcinoma, Thyroid: Off. J. Am. Thyroid Assoc. 24 (2) (2014) 232–240.
[21] G.M. Tozer, C. Kanthou, B.C. Baguley, Disrupting tumour blood vessels, Nature reviews, Cancer 5 (6) (2005) 423–435.
[22] D.W. Siemann, The unique characteristics of tumor vasculature and preclinical evidence for its selective disruption by Tumor-Vascular Disrupting Agents, Cancer Treat. Rev. 37 (1) (2011) 63–74.
[23] S.K. Libutti, L.B. Anthony, D.J. Chaplin, J.A. Sosa, A phase II study of combretastatin A4-phosphate (CA4P) in the treatment of well-differentiated, low- to intermediate-grade, unresectable, recurrent, or metastatic pancreatic, or GI neuroendocrine tumors/carcinoid (GI-NETs/PNETs) with elevated biomarkers, J. Clin. Oncol. 35 (4_suppl) (2017). 432-432.
[24] W. Song, Z. Tang, D. Zhang, X. Wen, S. Lv, Z. Liu, M. Deng, X. Chen, Solid tumor therapy using a cannon and pawn combination strategy, Theranostics 6 (7) (2016) 1023–1030.
[25] S.A. Lang, C. Moser, E.M. Jung, K. Pfister, E.K. Geissler, H.J. Schlitt, Effects of ASA404, a vascular disrupting agent, on tumor growth of gastric cancer in an experimental model, J. Clin. Oncol. 29 (4_suppl) (2011). 48-48.
[26] P.M. Lorusso, S.A. Boerner, S. Hunsberger, Clinical development of vascular disrupting agents: what lessons can we learn from ASA404?, Journal of clinical oncology : official journal of the American Society of, Clin. Oncol. 29 (22) (2011) 2952–2955.
[27] G.J. Madlambayan, A.M. Meacham, K. Hosaka, S. Mir, M. Jorgensen, E.W. Scott, D.W. Siemann, C.R. Cogle, Leukemia regression by vascular disruption and antiangiogenic therapy, Blood 116 (9) (2010) 1539–1547.
[28] Y.J. Ho, T.C. Wang, C.H. Fan, C.K. Yeh, Current progress in antivascular tumor therapy, Drug Discovery Today 22 (10) (2017) 1503–1515.
[29] L.P. Liu, R.L. Ho, G.G. Chen, P.B. Lai, Sorafenib inhibits hypoxia-inducible factor-1alpha synthesis: implications for antiangiogenic activity in hepatocellular carcinoma, Clin. Cancer Res.: An Off. J. Am. Assoc. Cancer Res. 18 (20) (2012) 5662–5671.
[30] B.J. Monk, L.E. Minion, R.L. Coleman, Anti-angiogenic agents in ovarian cancer: past, present, and future, Annals of oncology : official journal of the European Society for, Med. Oncol. 27 (Suppl 1) (2016) i33–i39.
[31] H. Wang, L. Zhou, K. Xie, J. Wu, P. Song, H. Xie, L. Zhou, J. Liu, X. Xu, Y. Shen, S. Zheng, Polylactide-tethered prodrugs in polymeric nanoparticles as reliable nanomedicines for the efficient eradication of patient-derived hepatocellular carcinoma, Theranostics 8 (14) (2018) 3949–3963.
[32] Q. Sun, X. Sun, X. Ma, Z. Zhou, E. Jin, B. Zhang, Y. Shen, E.A. Van Kirk, W.J. Murdoch, J.R. Lott, T.P. Lodge, M. Radosz, Y. Zhao, Integration of nanoassembly functions for an effective delivery cascade for cancer drugs, Adv. Mater. (Deerfield Beach, Fla.) 26 (45) (2014) 7615–7621.
[33] H. Kobayashi, R. Watanabe, P.L. Choyke, Improving conventional enhanced permeability and retention (EPR) effects; what is the appropriate target?, Theranostics 4 (1) (2013) 81–89
[34] S. Yang, H. Gao, Nanoparticles for modulating tumor microenvironment to improve drug delivery and tumor therapy, Pharmacol. Res. 126 (2017) 97–108.
[35] H. Gao, Shaping tumor microenvironment for improving nanoparticle delivery, Curr. Drug Metab. 17 (8) (2016) 731–736.
[36] W. Xiao, S. Ruan, W. Yu, R. Wang, C. Hu, R. Liu, H. Gao, Normalizing tumor vessels to increase the enzyme-induced retention and targeting of gold nanoparticle for breast cancer imaging and treatment, Mol. Pharm. 14 (10) (2017) 3489–3498.
[37] T. Liu, D. Zhang, W. Song, Z. Tang, J. Zhu, Z. Ma, X. Wang, X. Chen, T. Tong, A poly(l-glutamic acid)-combretastatin A4 conjugate for solid tumor therapy: Markedly improved therapeutic efficiency through its low tissue penetration in solid tumor, Acta Biomater. 53 (2017) 179–189.
[38] H. Yu, Z. Tang, D. Zhang, W. Song, Y. Zhang, Y. Yang, Z. Ahmad, X. Chen, Pharmacokinetics, biodistribution and in vivo efficacy of cisplatin loaded poly (L-glutamic acid)-g-methoxy poly(ethylene glycol) complex nanoparticles for tumor therapy, J. Control. Rel. Off. J. Control. Rel. Soc. 205 (2015) 89–97.
[39] J. Li, W. Xu, D. Li, T. Liu, Y.S. Zhang, J. Ding, X. Chen, Locally deployable nanofiber patch for sequential drug delivery in treatment of primary and advanced orthotopic hepatomas, ACS Nano 12 (7) (2018) 6685–6699.
[40] V. Sivalingam, R. McVey, K. Gilmour, S. Ali, C. Roberts, A. Renehan, H. Kitchener, E. Crosbie, A presurgical window-of-opportunity study of metformin in obesity-driven endometrial cancer, Lancet (London, England) 385 (Suppl 1) (2015) S90.
[41] J. Alsousou, M. Thompson, P. Harrison, K. Willett, S. Franklin, Effect of platelet-rich plasma on healing tissues in acute ruptured Achilles tendon: a human immunohistochemistry study, Lancet (London, England) 385 (Suppl 1) (2015) S19.
[42] S. Cuylen, C. Blaukopf, A.Z. Politi, T. Muller-Reichert, B. Neumann, I. Poser, J. Ellenberg, A.A. Hyman, D.W. Gerlich, Ki-67 acts as a biological surfactant to disperse mitotic chromosomes, Nature 535 (7611) (2016) 308–312.
[43] R. Altaha, M. Almubarak, M.D. Newton, A. Torres-Trejo, G. Marano, G. Hobbs, L. Gibson, W.P. Petros, S.C. Remick, A pilot study of fosbretabulin with bevacizumab in recurrent high-grade gliomas, J. Clin. Oncol. 28 (15_suppl) (2010). TPS147-TPS147.
[44] R. Gomez, Vascular disrupting and antiangiogenic agents: better together than on their own, Fertil. Steril. 100 (5) (2013) 1234–1235.
[45] S. Peng, Y. Wang, H. Peng, D. Chen, S. Shen, B. Peng, M. Chen, R. Lencioni, M. Kuang, Autocrine vascular endothelial growth factor signaling promotes cell proliferation and modulates sorafenib treatment efficacy in hepatocellular carcinoma, Hepatology (Baltimore, MD) 60 (4) (2014) 1264–1277.